Chapter 5

Semiconductor Optical Amplifier (SOA)–Based Amplification of Intensity-Modulated Optical Pulses — Deterministic Timing Jitter and Pulse Peak Power Equalization Analysis

T. Alexoudi, G.T. Kanellos, S. Dris, D. Kalavrouziotis, P. Bakopoulos, A. Miliou and N. Pleros

Additional information is available at the end of the chapter

http://dx.doi.org/10.5772/61712

Abstract

During the last few years, large-scale efforts towards realizing high-photonic integration densities have put SOAs in the spotlight once again. Hence, the need to develop a complete framework for SOA-induced signal distortion to accurately evaluate a system's performance has now become evident. To cope with this demand, we present a detailed theoretical and experimental investigation of the deterministic timing jitter and the pulse peak power equalization of SOA-amplified intensity-modulated optical pulses. The deterministic timing jitter model relies on the pulse mean arrival time estimation and its analytic formula reveals an approximate linear relationship between the deterministic timing jitter and the logarithmic values of intensity modulation when the SOA gain recovery time is faster than the pulse period. The theoretical analysis also arrives at an analytic expression for the intensity modulation reduction (IMR), which clearly elucidates the pulse peak power equalization mechanism of SOA. The IMR analysis shows that the output intensity modulation depth is linearly related to the respective input modulation depth of the optical pulses when the gain recovery time is faster than the pulse period. This novel theoretical platform provides a qualitative and quantitative insight into the SOA performance in case of intensity-modulated optical pulses.

Keywords: Deterministic timing jitter, Pulse peak power equalization, Intensity modulation reduction, Semiconductor optical amplifier, Modulation depth index

1. Introduction

Semiconductor optical amplifiers (SOAs) have long been the subject of considerable research interest, mainly exploiting their nonlinear properties to provide fast all-optical signal processing [1], such as high-speed wavelength conversion (WC) [2, 3], bitwise logic operations [4-6], and signal regeneration [7]. The broad-scale efforts towards realizing high photonic integration densities have, however, put the use of SOAs as amplification elements in the spotlight once again, since any alternative integrated amplifier competitor [8] lags far behind in terms of integration maturity. SOAs currently emerge as the preeminent on-chip amplifier solution and their reintroduction in the toolbox of the optical network designer is now evident in many key network subsystems. As a result, multiple demonstrations of SOAs performing as pure amplifier stages [9, 10] or as ON-OFF gating elements [11], where amplification occurs in the ON state, have been presented. Their ubiquitous use spans diverse network segments, enabling leading edge applications that extend from metro [11] to access network environments [10] and to on-chip or on-board datacom systems [9].

A concerted research effort on SOA-based devices, spanning the last 20 years, has unraveled most of their underlying amplification secrets, addressing a variety of linear and nonlinear phenomena and their impact on a system's performance [12]. Pulse-shaped asymmetry owing to SOA saturation effects, for example, has been one of the key findings and has been extensively studied for the past years [13]. However, it was only recently that a novel theoretical analysis correlated this behavior to SOA-induced deterministic timing jitter that optical pulses experience during the amplification process, also suggesting an analytic mathematical formula for its accurate estimation [14, 15]. On the other hand, amplitude modulation phenomena for SOA in-line amplification have been theoretically studied [16, 17] but the pulse peak power equalization properties of SOAs, although experimentally utilized in many cases [18–20], have never been expressed in an analytical form that would allow a straightforward estimation for any case of input signal. So far, the pulse peak power equalization properties of SOAs have been theoretically and experimentally investigated only for the SOA-based interferometric switches [20]. As a result, the proposed theoretical model cannot be applied for single SOA in-line amplification cases, since it relies on cross-phase modulation (XPM) phenomena that take place in SOA-based interferometric devices. Although research efforts have shed plenty of light on the SOA-based amplification process during the last few years, a complete framework for SOA-induced signal distortion in case of intensity-modulated optical pulses, including both deterministic timing jitter and the intensity modulation reduction analysis, is still missing.

In order to fill the current gap in the system's performance assessment, we present here a holistic theoretical analysis for the SOA-based amplification process along with its experimental verification when intensity-modulated optical pulses are inserted into the amplifier. The aim of this chapter is to provide a systematic methodology on the origin, nature and quantification of SOA-induced deterministic timing jitter and pulse peak power equalization that intensity-modulated optical pulses experience during the amplification process. At first, an analytic formula for the pulse mean arrival time at the SOA exit is derived, providing a comprehensive picture of jitter origin and allowing for reliable estimation of the deterministic

http://dx.doi.org/10.5772/61712

jitter induced during the SOA amplification. The theoretical analysis continues with an analytical mathematical expression of intensity modulation reduction induced by SOA amplification. More specifically, the output-versus-input modulation depth of the amplifier is examined for several saturation levels to thoroughly investigate the pulse peak power equalization capabilities of the SOA. The theoretical models are also experimentally verified with the obtained results proving good agreement between theory and experimental observations, in both cases. Moreover, the deterministic timing jitter analysis reveals an approximate linear relationship between jitter values and the logarithm of pulse peak power modulation. Both experimental and theoretical results show that deterministic timing jitter minimization can be achieved by operating the SOA in the strongly saturated region. On the other hand, pulse peak power equalization analysis indicates a linear dependence between the output and input modulation depth indices. In that case, results show that the amplifier yields higher intensity modulation reduction values when it is operated in the saturation regime and for increased SOA gain levels.

In this perspective, the following sections of the chapter have been organized so as to introduce the concept and provide the analytical theoretical framework of the SOA-induced deterministic timing jitter and the pulse peak power equalization properties for intensity-modulated optical pulses, as well as to describe the experimental setup along with the respective results obtained in each case and finally discuss potential extensions of the proposed theoretical models.

2. Concept and theoretical analysis

It is a well-known fact that intensity-modulated optical pulses will experience a pulse-shaped distortion and intensity modulation suppression when propagating through the SOA. The shift of the amplified pulse peak towards its rising edge owes to the higher gain that the leading edge of every incoming pulse experiences compared to the gain received by the trailing edge of the pulse [13]. This "center of gravity" deviation of the exiting optical pulse indicates a subsequent deviation of the mean pulse arrival time T_{MEAN} at the SOA exit. These systematic signal asymmetries originating from steeper and more gradual pulse edges are the root cause of the deterministic timing jitter depending on input data characteristics. When pulses of unequal peak power arrive at the input of the SOA, each pulse is displaced by a different amount resulting in a mean arrival time deviation at the output. Thus, when intensity-modulated pulses are injected into the SOA, and assuming the pulse period is greater than the SOA-gain recovery time, the different peak power levels will generate different dips in the SOA gain that cause different pulse shifts, leading to varying timing jitter values.

Apart from the peak position deviation of the optical pulses, SOAs can also induce pulse peak power equalization of incoming intensity-modulated optical pulses. This can, in turn, yield in a reduction in intensity modulation of the optical pulses at the SOA output. Assuming, again, that the SOA gain recovery time is faster than the pulse period, the pulse peak power equalization originates from the amplification dissimilarities arising between the low and high pulse

peak powers. A high gain is received by the lower peak-powered pulses whereas a lower gain is experienced by the higher peak-powered pulses, resulting in nearly power-equivalent amplified pulses obtained at the SOA exit. As a result, the modulation depth index of the input pulses will always be higher than the respective outputs of the amplifier pointing out an intensity modulation reduction of the exiting optical pulse stream.

The following analysis aims to provide a theoretical insight into the origin of the deterministic timing jitter and elucidate the pulse peak power equalization mechanism during the SOA amplification of intensity-modulated optical pulses. Considering the amplifier as a spatially concentrated device, the instantaneous amplifier gain $G(t)$ experienced by each pulse entering the SOA is expressed as [13, 20]:

$$G(t) = 1/\left[1-\left(1-1/G_0\right)\cdot\exp\left(-U_{\text{in}}(t)/U_{\text{sat}}\right)\right] \tag{1}$$

where G_0 represents the SOA steady-state gain and $U_{in}(t)$ the accumulated injected pulse energy given by:

$$U_{\text{in}}(t) = \int_{-\infty}^{t} P_{\text{in}}(t)\cdot dt \tag{2}$$

and the U_{sat} is the well-known saturation energy of the device. To this end, the output pulse exiting the SOA can be calculated as:

$$P_{\text{out}}(t) = P_{\text{in}}(t)\cdot G(t) \tag{3}$$

by defining $P_{\text{in}}(t)$ as the input pulse power.

2.1. Deterministic timing jitter analysis

Considering Gaussian pulses as input to the SOA, the input pulse power is defined as $P_{\text{in}}(t)=P_p\cdot\exp\left(-t^2/T_0^2\right)$ with peak power denoted as P_{p} and 1/*e* pulsewidth equal to T_0. The mean arrival time T_{MEAN} for every individual pulse is calculated [21, 22] as:

$$T_{\text{MEAN}} = \frac{\int_{-\infty}^{+\infty} t\cdot P_{\text{out}}(t)\cdot dt}{U_{\text{total}}} = \frac{\int_{-\infty}^{+\infty} t\cdot P_{\text{in}}(t)\cdot G(t)\cdot dt}{\int_{-\infty}^{+\infty} P_{\text{in}}(t)\cdot G(t)\cdot dt} = \frac{A}{B} \tag{4}$$

where U_{total} is the total output pulse energy. By replacing $P_{\text{in}}(t)$ and $G(t)$ with their respective expressions, we obtain *A* and *B* in Eq. (5) and Eq. (6), respectively.

http://dx.doi.org/10.5772/61712

$$A = \int_{-\infty}^{+\infty} t \cdot P_{\mathrm{p}} \cdot \exp\left(-\frac{t^2}{T_0^2}\right) \cdot \left[1 - \left(1 - \frac{1}{G_0}\right) \cdot \exp\left(\frac{-P_{\mathrm{p}} \cdot \int_{-\infty}^{t} \exp\left(-\frac{t^2}{T_0^2}\right) \cdot dt}{U_{\mathrm{sat}}}\right)\right]^{-1} \cdot dt \tag{5}$$

$$B = \int_{-\infty}^{+\infty} P_{\mathrm{p}} \cdot \exp\left(-\frac{t^2}{T_0^2}\right) \cdot \left[1 - \left(1 - \frac{1}{G_0}\right) \cdot \exp\left(\frac{-P_{\mathrm{p}} \cdot \int_{-\infty}^{t} \exp\left(-\frac{t^2}{T_0^2}\right) \cdot dt}{U_{\mathrm{sat}}}\right)\right]^{-1} \cdot dt \tag{6}$$

By expanding $G(t)$ both in the numerator A and in the denominator B in a first-order Taylor series around the center position of the pulse at $t=0$, after some algebra, Eq. (4) becomes:

$$T_{\mathrm{MEAN}} = -\frac{T_0^2 \cdot \left(1 - \frac{1}{G_0}\right) \cdot \left[\frac{P_{\mathrm{p}}}{U_{\mathrm{sat}}} \cdot \exp\left(-\frac{P_{\mathrm{p}}}{U_{\mathrm{sat}}} \cdot \frac{T_{0 \cdot \sqrt{\pi}}}{2}\right)\right]}{2 \cdot \left[1 - \left(1 - \frac{1}{G_0}\right) \cdot \exp\left(-\frac{P_{\mathrm{p}}}{U_{\mathrm{sat}}} \cdot \frac{T_0 \cdot \sqrt{\pi}}{2}\right)\right]} \tag{7}$$

Eq. (7) determines the mean arrival time T_{MEAN} of every pulse as a function of its peak power, its time duration and of the SOA steady-state gain. In Figure 1, the T_{MEAN} quantity is illustrated versus a pulse peak power range of 0 mW to 20 mW, for three different SOA gain G_0 values and a pulsewidth of 20 ps. As the center of the pulse is assumed to be at $t=0$, the time shift induced by SOA amplification process will always be leftward. As a consequence, T_{MEAN} will always be a negative quantity that will continuously decrease until reaching a saturation plateau [15].

In addition, according to Figure 1, the steepness of the slope of the T_{MEAN} curve indicated two distinct areas for the T_{MEAN} based on the peak power: area A, corresponding to the nonsaturated SOA gain regime, where the SOA still responds radically to input peak power resulting in enhanced timing jitter values for the amplified pulses, and area B, where the SOA operates in its strongly saturated gain region. In the last case, the curve of T_{MEAN} decreases smoothly, mitigating in this way the differences of mean arrival time T_{MEAN} compared to SOA operation in area A and leading to lower timing jitter values [15].

The monotonic slope of mean arrival time T_{MEAN} implies that the lowest and highest values are obtained for the corresponding lowest and highest peak power input pulses [15]. In case the P_{p} values are within a finite set between minimum and maximum values, the peak-to-peak

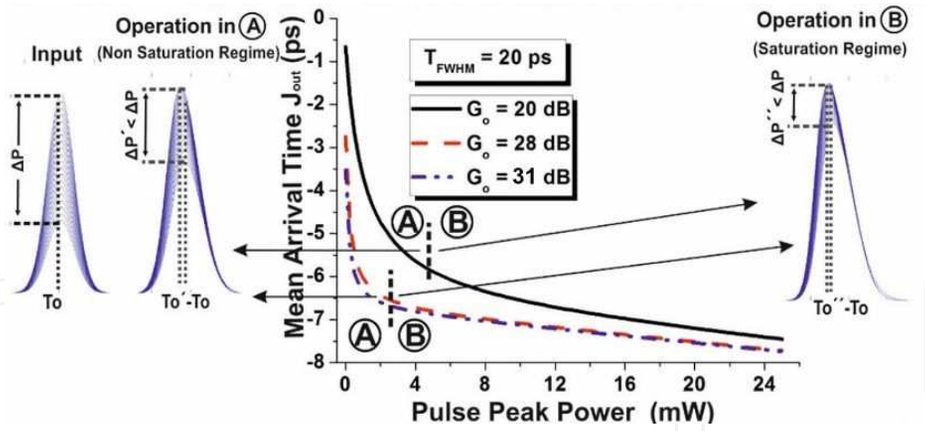

Figure 1. Theoretical mean arrival time (T_{MEAN}) vs. pulse peak power values. Insets of the figure show the eyediagrams of a jitter-free intensity-modulated signal before entering the SOA amplifier and the output signals when the SOA operates in the nonsaturation (area A) and in the strongly saturated regime (area B), respectively.

deterministic timing jitter is determined as the difference between the respective minimum and maximum mean arrival time values T_{MEAN} [15], as shown in Eq. (8):

$$J_{\mathrm{pp}}^{D} = T_{\mathrm{MEAN}}^{\max} - T_{\mathrm{MEAN}}^{\min} \tag{8}$$

where $T_{\mathrm{MEAN}}^{\min} = T_{\mathrm{MEAN}}\left(P_{\mathrm{p}}^{\min}\right)$ and $T_{\mathrm{MEAN}}^{\max} = T_{\mathrm{MEAN}}\left(P_{\mathrm{p}}^{\max}\right)$.

An interesting conclusion for deterministic timing jitter can be drawn by expressing the peak power P_{p} in logarithmic instead of linear scale. Figure 2 is a graphical representation of Eq. (7), showing the dependence of T_{MEAN} on peak power values, when the latter is expressed in dBm. As illustrated, the curved sections for peak power values lower than –5 dBm, and higher than 0 dBm can be very well approximated by second-degree polynomials.

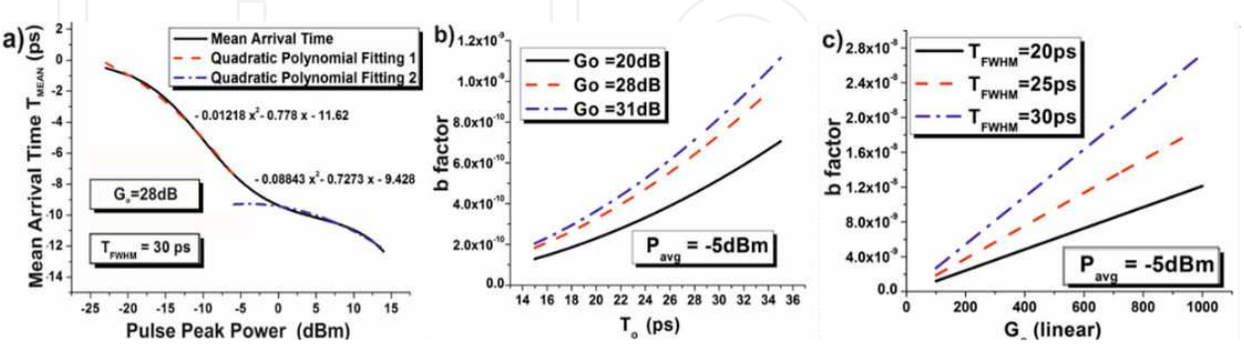

Figure 2. a) Mean arrival time (T_{MEAN}) vs. pulse peak power expressed in dBm for Go = 28 dB and 30-ps-long pulses. Dashed lines denote the fit of T_{MEAN} with second-degree polynomials. Linearity of deterministic timing jitter denoted by b factor of Eq. (12) versus (b) 1/e pulsewidth and (c) SOA gain levels, showing the dependence of T_{MEAN} on peak power values, the latter expressed in dBm.

http://dx.doi.org/10.5772/61712

Thus, Eq. (7) can be expanded into a second-order Taylor series around a reference peak power P_{REF}, again expressed in dBm. Moreover, by substituting in Eq. (8), the values of T_{MEAN} corresponding to the highest and lowest peak power pulses $P_{\mathrm{p}}^{\max}$(dBm) and $P_{\mathrm{p}}^{\min}$(dBm), respectively, the deterministic timing jitter can now be written as shown in Eq. (9):

$$J_{P_{\mathrm{p}}}^{D}=\frac{1}{2!}\cdot a\cdot\left[\left(P_{\mathrm{p}}^{\max}\left(\mathrm{dBm}\right)-P_{\mathrm{REF}}\left(\mathrm{dBm}\right)\right)^{2}-\left(P_{\mathrm{p}}^{\min}\left(\mathrm{dBm}\right)-P_{\mathrm{REF}}\left(\mathrm{dBm}\right)\right)^{2}\right]+b\cdot\left(P_{\mathrm{p}}^{\max}\left(\mathrm{dBm}\right)-P_{\mathrm{p}}^{\min}\left(\mathrm{dBm}\right)\right) \tag{9}$$

where $a=\frac{d^{2}J_{p_p}^{D}}{dP^{2}}\Big|_{P=P_{REF\,(dBm)}}$ and $\mathrm{b}=\frac{dJ_{p_p}^{D}}{dP}\Big|_{P=P_{REF\,(dBm)}}$ Eq. (9) can be further simplified using some straightforward algebra into:

$$J_{p_{\mathrm{p}}}^{D}=\frac{1}{2!}\cdot a\cdot\Delta P\left(\mathrm{dB}\right)\cdot\left[P_{\mathrm{p}}^{\max}\left(\mathrm{dBm}\right)+P_{\mathrm{p}}^{\min}\left(\mathrm{dBm}\right)-2\cdot P_{\mathrm{REF}}\left(\mathrm{dBm}\right)\right]+b\cdot\Delta P\left(\mathrm{dB}\right) \tag{10}$$

where $\Delta P=P_{\mathrm{p}}^{\max}-P_{\mathrm{p}}^{\min}$ is the intensity modulation expressed in dB. By selecting the P_{REF}(dBm) value to be the mid-point between the minimum $P_{\mathrm{p}}^{\min}$ and maximum $P_{\mathrm{p}}^{\max}$ peak power level, so that $P_{\mathrm{p}}^{\max}(\mathrm{dBm})=P_{\mathrm{REF}}(\mathrm{dBm})+\Delta P(dB)/2$. and $P_{\mathrm{p}}^{\min}(\mathrm{dBm})=P_{\mathrm{REF}}(\mathrm{dBm})-\Delta P(\mathrm{dB})/2$, the quantity contained in the brackets becomes zero and the deterministic timing jitter expression turns into:

$$J_{\mathrm{p}_p}^{\mathrm{D}}=b\cdot\Delta P\left(\mathrm{dB}\right) \tag{11}$$

This formula reveals a linear relationship between deterministic timing jitter and intensity modulation with the linearity factor b provided by Eq. (12).

$$\begin{aligned}&-T_0^2\cdot e^{\frac{P_{\mathrm{REF}}\left(\mathrm{dBm}\cdot 10^{-3}\right)}{10}}\cdot\left(G_0-1\right)\cdot\\&\cdot\left(2\cdot G_0-2\cdot G_0\cdot e^{\frac{T_0\cdot\sqrt{\pi}\cdot U_{\mathrm{sat}}\cdot e^{\frac{P_{\mathrm{REF}}\left(\mathrm{dBm}\cdot 10^{-3}\right)}{10}}}{2}}+G_0\cdot T_0\cdot\sqrt{\pi}\cdot U_{\mathrm{sat}}\cdot e^{\frac{P_{\mathrm{REF}}\cdot\left(\mathrm{dBm}\cdot 10^{-3}\right)}{10}+\frac{T_0\cdot\sqrt{\pi}\cdot U_{\mathrm{sat}}\cdot e^{\frac{P_{\mathrm{REF}}\left(\mathrm{dBm}\cdot 10^{-3}\right)}{10}}}{2}}-2\right)\cdot\\&\cdot\left(40\cdot U_{\mathrm{sat}}\cdot\left(G_0\cdot e^{\frac{T_0\cdot\sqrt{\pi}\cdot U_{\mathrm{sat}}\cdot e^{\frac{P_{\mathrm{REF}}\left(\mathrm{dBm}\cdot 10^{-3}\right)}{10}}}{2}}-G_0+1\right)^{2}\right)^{-1}\end{aligned} \tag{12}$$

By plotting Eq. (12) for different pulsewidths and SOA gain levels as shown in Figure 2(b) and in Figure 2(c), respectively, the absolute value of b increases with T_0 and G_0 for a given P_{REF} (dBm) value. This indicates that higher jitter values are obtained for higher pulsewidths and higher SOA gains when the same intensity modulation level and the same P_{REF} (dBm) values are used.

2.2. Pulse peak power equalization analysis

By defining T as the bit period, P_p as the average peak power value across the whole control signal sequence, Ω as the modulation frequency and m as the modulation depth index, the peak power of each k-th individual pulse of an intensity-modulated clock pulse sequence entering the SOA is given by $P_{\mathrm{p}}^{k} = P_{\mathrm{p}} \cdot [1 + m \cdot \cos(\Omega \cdot k \cdot T)]$. Since multilevel clock puls are considered to enter the SOA as input, the modulation depth index can be determined by their discrete levels. By substituting the intensity-modulated clock pulse sequence P_{p}^{k} in (2), $U_{\mathrm{in}}(t)$ is transformed as follows:

$$U_{\mathrm{in}}\left(t\right) = \int_{-\infty}^{t} P_{\mathrm{in}}\left(t\right) \cdot dt = P_{\mathrm{p}} \cdot \left(1 + m \cdot \cos\left(\Omega \cdot k \cdot T\right)\right) \cdot \int_{-\infty}^{t} a\left(t'\right) \cdot dt' \tag{13}$$

where $a(t')$ denotes the pulse waveform. Eq. (1) shows that the gain saturates to a minimum value until the whole pulse energy has passed through the amplifier. However, it is assumed that the gain recovers back to its steady-state value before the next pulse enters the amplifier. As a result, Eq. (1) is valid for the whole bit sequence, allowing in this way for the replacement of the time-dependent integral $\int a(t') \cdot dt'$ contained in Eq. (13) with a time-independent constant value A that corresponds to the total area contained in the pulse waveform [20]. To this end, the output intensity-modulated clock pulse sequence $P_{o/p}$ after using Eq. (1) and Eq. (13) can be expressed as follows:

$$P_{o/p}\left(m\right) = \frac{P_p \cdot \left(1 + m \cdot \cos\left(\Omega \cdot k \cdot T\right)\right)}{\left[1 - \left(1 - \left(1/G_0\right)\right) \cdot \exp\left(-P_p \cdot \left(1 + m \cdot \cos\left(\Omega \cdot k \cdot T\right)\right) \cdot A / U_{\mathrm{sat}}\right)\right]} \tag{14}$$

Eq. (14) depicts that $P_{o/p}$ is a function of the SOA gain G_0, the saturation energy U_{sat} and the pulse peak power $P_0 \cdot (1 + m \cdot \cos(\Omega \cdot k \cdot T))$. By expanding (14) in a first-order Taylor series around $m = 0$ the output pulse peak power can be written as the sum of a dc signal component and an oscillation term ac at Ω:

$$P_{p/o}\left(m\right) = P_{o/p}\Big|_{m=0} + \left.\frac{\partial P_{o/p}}{\partial m}\right|_{m=0} \cdot m \tag{15}$$

http://dx.doi.org/10.5772/61712

where the *dc* component is expressed as shown in (16):

$$P_{o/p}\Big|_{m=0} = \frac{P_p}{1-\left(1-\frac{1}{G_0}\right)\cdot exp\left(-\frac{P_p\cdot A}{U_{sat}}\right)} \tag{16}$$

and the *ac* component as

$$\frac{\partial P_{o/p}}{\partial m}\Big|_{m=0} = \left[\frac{P_p}{1-\left(1-\frac{1}{G_0}\right)\cdot exp\left(-\frac{P_p\cdot A}{U_{sat}}\right)} - \frac{P_p\cdot\left(1-\frac{1}{G_0}\right)\cdot\frac{P_p\cdot A}{U_{sat}}\cdot exp\left(-\frac{P_p\cdot A}{U_{sat}}\right)}{\left[1-\left(1-\frac{1}{G_0}\right)\cdot exp\left(-\frac{P_p\cdot A}{U_{sat}}\right)\right]^2}\right]\cdot\cos\left(\Omega\cdot k\cdot T\right) \tag{17}$$

Dividing all terms of Eq. (15) by the *dc* component, we can calculate the modulation depth index at the output by dividing Eq. (17) by Eq. (16) and then multiplying by *m*, as shown in (18):

$$m_{o/p} = \left[ac\left(\text{component}\right)/dc\left(\text{component}\right)\right]\cdot m \tag{18}$$

Finally, the modulation depth index of the output pulse peak power $m_{o/p}$ is found to be:

$$m_{o/p} = \frac{1-\left(1-\frac{1}{G_0}\right)\cdot\exp\left(-\frac{P_p\cdot A}{U_{\text{sat}}}\right)\cdot\left(1+\frac{P_p\cdot A}{U_{\text{sat}}}\right)}{1-\left(1-\frac{1}{G_0}\right)\cdot\exp\left(-\frac{P_{p\cdot A}}{U_{\text{sat}}}\right)}\cdot m \tag{19}$$

Eq. (19) provides a complete description of the SOA amplifier response to an injected intensity-modulated clock pulse sequence. It shows that the intensity modulation at the output is linearly related to the intensity modulation at the input and that the constant of proportionality depends on the SOA steady-state gain G_0, the average peak power P_{p} and the saturation energy U_{sat}. In addition, the intensity modulation always decreases at the output of the amplifier. To relate the input and output intensity modulation indices *m* and $m_{o/p}$ respectively, we define the Intensity Modulation Reduction (IMR) index as

$$\text{IMR} = 10\cdot\log\left|m_{o/p}/m\right| \tag{20}$$

Given that the intensity modulation depth indices m and $m_{o/p}$ of the input and the amplified output pulses are in principle the amplitudes of a slow varying frequency component at Ω inducing the power fluctuations on the pulses [20], Eq. (20) indicates the Intensity Modulation Reduction (IMR) of this frequency component after the SOA amplification process. In specific, the $m_{o/p}$ power level at the SOA's exit will be reduced from its respective power level at the input m by an amount equal to the IMR value.

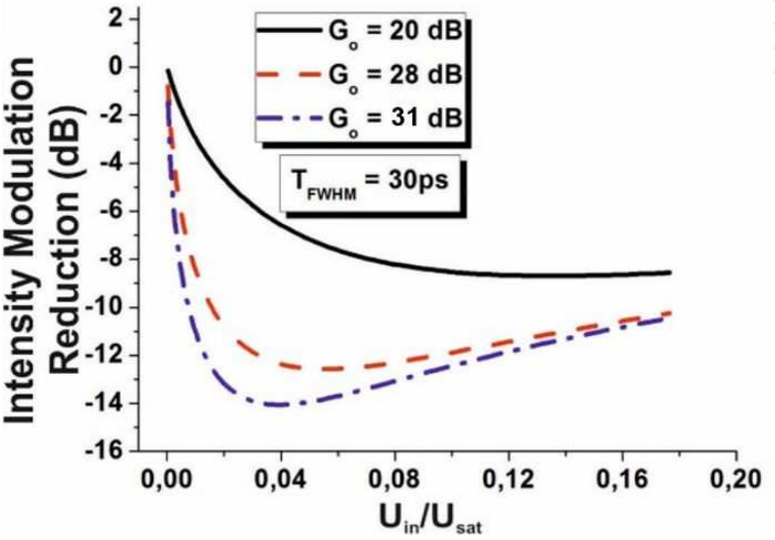

Figure 3. Theoretical Intensity Modulation Reduction (IMR) expressed in dB vs. U_{in}/U_{out} values. IMR is illustrated for different SOA gain levels in the case of 30-ps-long pulses.

Figure 3 depicts the graphical representation of Eq. (20) for different SOA gains versus U_{in}/U_{sat} quantity. The values of IMR represent a negative quantity since the output modulation depth is always smaller than the respective values at the input. A rapid drop of IMR leading to enhanced intensity modulation suppression is illustrated in Figure 3, when U_{in}/U_{sat} is almost 0.04 and the pulsewidth is equal to 30 ps for all SOA gain levels. Figure 3 shows that when SOA operates in low gain level corresponding to a gain value of 20 dB, a nearly constant IMR of 8 dB is obtained. However, for higher gains, the IMR increases to reach 14 dB for a SOA gain of 31 dB. In addition, the maximum intensity modulation reduction for a SOA gain value equal to 31 dB is achieved when U_{in}/U_{sat} quantity takes values between 0.01 and 0.05, implying that the SOA is capable of suppressing a large power variation at its input. As U_{in} increases, the IMR curves present a flat form and it is clamped to a constant level irrespective of the inserted pulse energy, after this specific U_{in} threshold.

3. Experiment and results

The scope of this section is to provide experimental verification of the theoretical analysis for the deterministic timing jitter and the intensity modulation reduction induced by the SOA

http://dx.doi.org/10.5772/61712

amplification process. Figure 4 demonstrates the experimental setup that was used for measurements with different pulsewidths and SOA gain levels. It consists of a 1549.2 nm mode-locked laser (TMLL) and a Ti:LiNbO-3 electro-optic modulator (MOD) driven by a 10 Gb/s pattern of alternating "1"s and "0"s, to create clock pulses at 5 GHz, so as to ensure a pulse period greater than the SOA gain recovery time (160 ps 1/e).

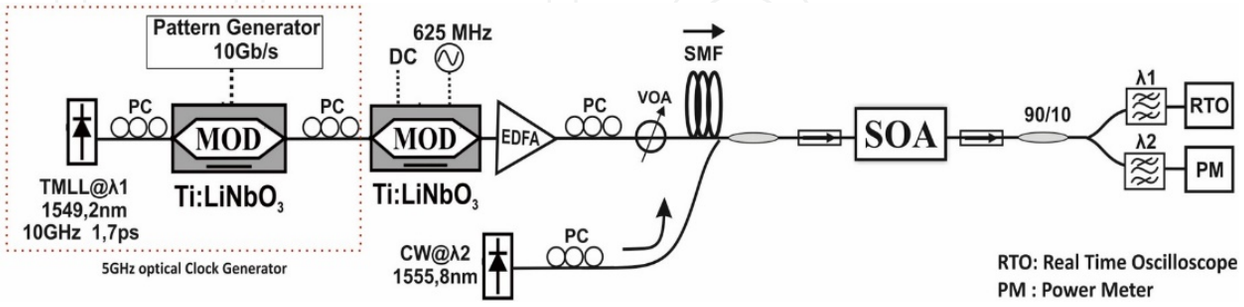

Figure 4. Experimental setup used for the deterministic timing jitter and intensity modulation reduction measurements.

In order to create an intensity-modulated pulse sequence, the clock signal is then injected into a second modulator driven by a 625 MHz sinusoidal signal that creates pulses with 8 different pulse peak power levels. The intensity-modulated clock signal is amplified via an erbium doped fiber amplifier (EDFA) in order to compensate the losses and properly adjust the required power levels of optical pulses before their introduction into the SOA. Two fiber spools of 800 m and 1225 m were employed to enable pulsewidth adjustment at 20 ps and 30 ps by exploiting the fiber dispersion. An additional CW beam at 1558.2 nm was utilized to adjust SOA gain level and as such to determine its operational regime. After setting the SOA gain to the desired value, the output pulse train was captured on a real-time oscilloscope with 16 GHz bandwidth and a jitter measurement floor of 300 fs, where the jittery pulses were collected for offline postprocessing. The experimental setup of Figure 4 was also used in order to experimentally verify the IMR graphs shown in Figure 3. By varying the CW signal inserted into the SOA in order to cover a broad operational SOA gain regime, the intensity modulation of the input signal, defined as the highest to the lowest pulse peak power ratio, was measured at the output of the SOA. The operation of the amplifier both in the nonsaturated regime and in the saturated regime was also ensured by properly adjusting the input signal power. By calculating the difference between the initial and the output modulation depth values, the experimental data of IMR for every different SOA gain level was obtained. The control and input signals were adjusted in terms of power and polarization by means of variable optical attenuators (VOA) and polarization controllers (PC). The SOA module was a 1.5-mm-long multiquantum well structure with a small signal gain of 31 dB. The device was driven at 450 mA and the U_{sat} parameter of the SOA was found to be approximately 7 fJ. The jittery pulses that were captured on the real-time oscilloscope at 100 GSa/s for offline postprocessing. The collected optical pulses were reconstructed with a sample time resolution of $\Delta t = 1.25$ ps, after 8-fold upsampling. For each run, the total output timing jitter, referred to as J^{TOTAL}, was calculated over

8192 pulses by means of Eq. (4) [15]. The total output timing jitter referred as J^{TOTAL} consists of noise-induced random jitter and deterministic jitter [23]. The deterministic timing jitter stems from pulse edge variations depending on the input data characteristics. On that account, it is crucial to separate the stochastic contribution of random jitter from the deterministic process that is only responsible for timing variations proportional to the pulses' intensity modulation. Thus, deterministic jitter is calculated as a peak-to-peak value (J_{pp}^{D}) between a minimum and a maximum value since a probabilistic distribution cannot be applied. On the contrary, random jitter is determined as the root-mean-square (rms) value of a normal distribution (J_{pp}^{R}). By using well-known equations of converting the root-mean-square (rms) to peak-to-peak values [24, 25] the total timing jitter J^{TOTAL} can be finally calculated as the following:

$$J^{\mathrm{TOTAL}} = J_{\mathrm{pp}}^{R} + J_{\mathrm{pp}}^{D} \tag{21}$$

The total timing jitter at the output of the SOA in the absence of pulse peak power variations is uncorrelated to the timing jitter induced from an intensity-modulated pulse sequence [15]. As such, it represents the accumulated random timing jitter of our experimental system:

$$J_{\mathrm{pp}}^{R} = J^{\mathrm{TOTAL}}\Big|_{\text{intensity modulation}=0\ \mathrm{dB}} \tag{22}$$

Based on this assumption, the deterministic timing jitter induced by the SOA amplification process can be calculated by subtracting the random jitter measurement floor from J^{TOTAL} when the input pulse sequence has a given intensity modulation [15]. Table 1 summarizes the timing jitter values for power-equalized pulses when the pulsewidth values are 20 ps and 30 ps and the SOA gains equal to 20 dB and 31 dB, respectively.

SOA Input				**SOA Output**	
Pulsewidth (ps)	**Random Jitter (ps)**		**Gain (dB)**	**Random Jitter Floor J_{PP}^{R} (ps)**	
Nonsaturation	Saturation				
20	J_{rms}^{R}	0.585	20	4.356	4.391
30		0.634		5.065	5.180
20	J_{PP}^{R}	4.048	31	6.082	4.223
30		4.460		6.596	5.779

Table 1. Timing jitter values for power-equalized pulses at the input and at the output of the SOA

http://dx.doi.org/10.5772/61712

3.1. Deterministic timing jitter: Theoretical and experimental results

Figure 5(a) and 5(b) show the eyediagrams of a 10 dB intensity-modulated input signal with 20 ps and 30 ps pulsewidths, respectively. Figure 5(c) and 5(d) depict the output eyediagrams for the two pulsewidths when the amplifier operates in the nonsaturated regime. Figure 5(e) and 5(f) illustrate similar results for the two pulsewidths in case the SOA is operated in the strongly saturated gain region. The experimental average peak power values for the eyediagrams obtained in Figure 5 are shown in Table 2. In the eyediagrams of Figure 5(c–f), the deterministic jitter is masked under the contribution of total jitter including the accumulated random jitter of the system as well. The irregular shapes of the output eye diagrams reveal, however, the pulse shape distortion that triggers the deterministic timing jitter.

SOA Gain	20 dB	
Pulsewidth	**Nonsaturated**	**Saturated**
20 ps	30 μW	1.85 mW
30 ps	34 μW	1.23 mW

Table 2. Experimental values for the obtained SOA eyediagrams in Figure 5.

Figure 5(g–j) depicts the experimental and theoretical results of the deterministic timing jitter versus input signal intensity modulation expressed in dB, for different gain levels, saturation regimes of the SOA and pulsewidths.

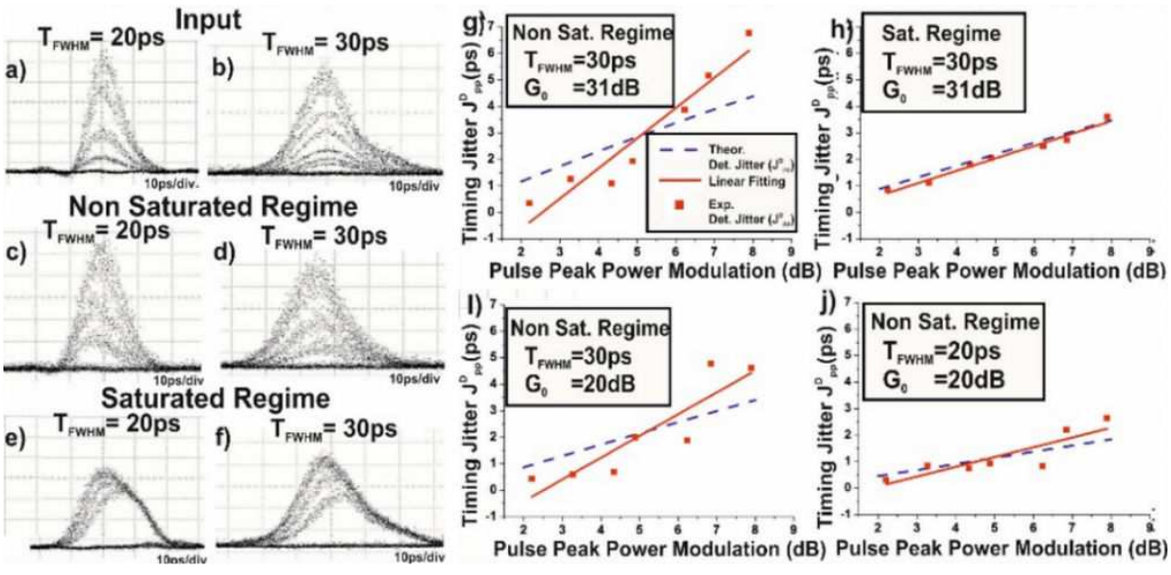

Figure 5. (a), (b) Eyediagram of an input optical signal with 10 dB intensity modulation with a pulsewidth of (a) 20 ps and (b) 30 ps, and the respective SOA output when the amplifier operates in the (c), (d) nonsaturated and (e),(f) strongly saturated regimes. The SOA gain level is equal to 20 dB for (a–f). Timescale for (a–f): 10 ps/div. Experimental and theoretical results for the deterministic timing jitter vs. pulse peak power modulation (intensity modulation) expressed in dB, for 30 ps pulsewidth and 31 dB SOA gain in (g) nonsaturated and (h) strongly saturated regimes, and for 20 dB SOA gain and nonsaturated region with (i) 30 ps and (j) 20 ps pulsewidths, respectively.

According to Eq. (11), the theoretical deterministic timing jitter depends linearly on intensity modulation levels. On that account, a linear fit was applied to the experimental data revealing good agreement between theoretical and experimental results obtained in all cases [15]. Figure 5(g) and (h) show theoretical deterministic timing jitter results obtained by applying Eq. (7) into Eq. (8), as well as the experimental data with their linear fit for 30 ps pulsewidth and 31 dB SOA gain level. The average pulse peak power values used in this case were 11 μW and 235 μW for unsaturated and saturated SOA operations, respectively. The graphs reveal a reduction of deterministic timing jitter in excess of 25% for the case of the SOA saturated operational regime. Figure 5(i) illustrates deterministic timing jitter evolution versus intensity modulation levels for 20 dB SOA gain using an average pulse peak power value of 34 μW. When compared with Figure 5(g), a decrease of the deterministic timing jitter values with the SOA gain level is evident. Finally, Figure 5(i) and 5(j) depict the deterministic timing jitter results for 30 ps and 20 ps pulsewidths, respectively, when all other operating parameters are the same, confirming that shorter pulses generate lower deterministic timing jitter levels [30 W average pulse peak power values for Fig. 5(j)]. In all cases, good qualitative and quantitative agreement between experiment and theory was achieved retaining the same deterministic timing jitter trend.

3.2. Intensity modulation reduction: Theoretical and experimental results

Figure 6 depicts the theoretical and experimental results for the output $m_{o/p}$ versus the input m modulation depth indices and the $m_{o/p}/m$ versus the input pulse energy U_{in} of optical pulses inserted in the SOA. The theoretical curves are denoted by solid lines, and the experimental observations by bullets. A linear fit was also applied to the experimental data in Figure 6(a), 6(b) and 6(d), due to the linear nature of the IMR indicated by Eq. (19) and it is represented by a dashed line. As can be noticed in Figure 6(a) and 6(b), the output modulation depth index depends linearly on the input modulation depth index when the SOA gain levels equal to 20 dB and 28 dB, respectively. In both cases, the amplifier operates in the nonsaturated region with the U_{in} values reaching up to 5 fJ and 0.5 fJ, respectively. Figure 6(c) demonstrates the $m_{o/p}/m$ ratio versus the input pulse energy U_{in} for SOA gain levels of 20 dB, 28 dB and 31 dB. As the gain level rises from 20 dB to 31 dB, the steepness of the slope increases and the curve shifts closer to the axis. In the case of gain equal to 31 dB, both unsaturated and saturated SOA experimental observations are shown in Figure 6(d) revealing higher intensity modulation reduction for strongly saturated SOA with the U_{in} reaching 2 fJ. Figure 6(d) presents in detail the output $m_{o/p}$ versus the input m modulation indices for the two operational SOA regimes for 31 dB gain level. The U_{in} value is directly associated to the SOA operational regime and imposes the slope of the $m_{o/p}$ versus m curve resulting in low or high variation between input and output modulation depth that in turn yields low- or high-intensity modulation reduction values. It can be observed that the slope of the curve is smaller in the case of a saturated SOA corresponding to U_{in} equal to 2 fJ in comparison with the unsaturated SOA referring to a U_{in} value equal to 0.2 fJ.

http://dx.doi.org/10.5772/61712

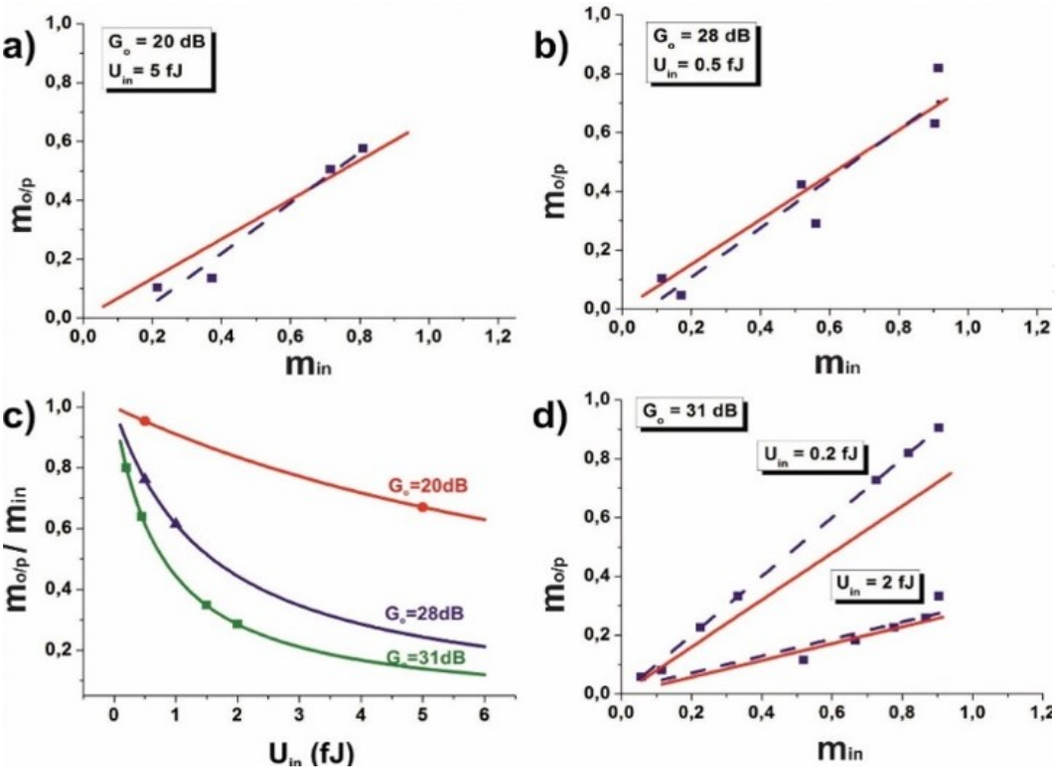

Figure 6. (a), (b) and (d) experimental and theoretical results for output modulation depth index versus input modulation depth index of intensity-modulated optical pulses for G_0=20dB, G_0 =28dB and G_0=31dB of the SOA. (d) Results in both nonsaturation and saturation regime of the SOA and (c) intensity modulation reduction ($m_{o/p}/m_{in}$) for the three SOA gain levels vs. U_{in}. In all cases, the bullets represent experimental measurements, the solid lines the respective theoretical curves and the dashed lines the experimental fit.

Comparison between dashed and solid lines in Figure 6(a–d) shows good agreement between theory and experiment and indicates the SOA potential to provide increased pulse peak power equalization at its output, when operating the amplifier in the saturation regime.

4. Discussion

The theoretical framework and its experimental verification for both deterministic timing jitter and intensity modulation reduction analysis have relied on the assumption that every pulse experiences the same initial steady-state gain. This assumption allowed for the treatment of the pulse sequence on a per pulse basis and for the use of clock pulses for its experimental validation. However, the theoretical analysis presented here can also be extended towards calculating both these phenomena, in the case of random data patterns with intensity-modulated pulses used as the input signal in SOAs.

In the case of deterministic timing jitter, when the SOA gain recovery time is faster than the bit period, all the incoming data pulses will again experience the same steady-state gain G_0 inside the amplifier. This condition allows Eq. (7) of the mean arrival time T_{MEAN} to be valid. But even if the SOA gain recovery time is slower than the bit period, Eq. (7) can be exploited

for calculating the mean arrival time T_{MEAN} of the data pulses and, subsequently, the deterministic timing jitter. In this case, the use of a random incoming data pattern into the SOA will actually result in different gain levels experienced by every individual optical pulse. On that account, G_0 should then be treated as an additional variable in Eq. (7) with its values residing within a certain range ΔG_0. This actually turns relationship (7) into a two-variable function, assuming a given pulsewidth and a constant U_{sat} parameter [15].

According to Figure 1, the same pulse peak power level results in a lower absolute value for the pulse mean arrival time when a lower gain value is perceived by the pulse. In Figure 1, for example, the absolute value of T_{MEAN} for a gain of 20 dB is always lower than the respective value for a SOA gain of 28 dB, which in turn is always lower than the respective value for a 30 dB SOA gain. This indicates that the deterministic jitter in case of different gain levels perceived by every pulse, as will be the case with random incoming data patterns and gain recovery times slower than the bit period, will be always slightly higher compared to the deterministic jitter values induced by the same pulse sequence when the SOA gain recovery time is faster than the bit period. For example, when the incoming data pulse with the lowest peak power level enters the amplifier after a long sequence of "1"s, it experiences the lowest SOA gain among all data pulses yielding, in this way, the lowest absolute value for its mean arrival time at the SOA output. At the same time, the highest data pulse comes after a long sequence of "0"s, so that it actually experiences the full gain of the amplifier, resulting in the highest absolute value among all data pulses for its mean arrival time T_{MEAN}. This scenario can certainly occur when a truly random data pattern with an intensity modulation that follows a certain statistical distribution will be injected into the SOA [15]. To this end, Eq. (7) indicates that higher deterministic timing jitter values should be expected in this case.

Following the same rationale, Eq. (19) of the modulation depth index of the output pulse peak power $m_{o/p}$ can also turn into a two-variable function (G_0, P_p) for a certain pulse waveform A and a constant U_{sat} parameter. In this way, it enables its utilization in cases of random data pattern when the SOA gain recovery time is greater than the bit period. Again, the worst-case scenario in terms of the intensity modulation level of the output pulses will take place when the pulses with the smallest peak power level follow a long sequence of "1"s and the pulses with the highest peak power level come after a long sequence of "0"s. The smallest pulses will experience the lowest gain while the highest pulses will perceive the full gain of the amplifier resulting in a less optimal peak power equalization compared to the respective case where the SOA gain recovers, and all pulses receive the same steady-state gain G_0. In such a traffic scenario, the random data pattern will limit the power equalization dynamics of the SOA, since the bit randomness will affect its ability to provide the same gain to every pulse and will lead to varying gain values that will be imprinted on the amplified optical pulses.

5. Conclusion

Research interest in semiconductor optical amplifiers (SOAs) has been lately renewed since SOAs appear as the most preferable on-chip amplifier option in many key network subsystems.

http://dx.doi.org/10.5772/61712

Although a concerted research effort on SOA-based devices spanning the last 20 years, has revealed most of their underlying amplification secrets, SOA effects on intensity-modulated optical pulses in terms of timing jitter and pulse peak power equalization have not yet been consolidated in a detailed analytical framework. On that account, we have presented in this chapter, a holistic theoretical framework verified by experimental results that establishes for the first time a systematic methodology for the deterministic timing jitter and peak power equalization estimation in case of intensity-modulated optical pulses entering the SOA. Experimental and theoretical results reveal a linear relationship between deterministic timing jitter and intensity modulation levels when the SOA gain recovery time is shorter than the bit period. The pulse mean arrival time is calculated as a function of the pulse peak power, the pulsewidth and the SOA steady-state gain. In addition, pulse peak power equalization analysis shows that intensity modulation at output is linearly related to the intensity modulation at the input and the constant of proportionality depends on the SOA steady-state gain G_0, the pulse peak power P_p and the saturation energy U_{sat}. Both deterministic timing jitter and intensity modulation reduction formulas derived in the proposed theoretical analysis, enable a qualitative and quantitative insight into the SOA performance when intensity-modulated optical pulses are inserted into the amplifier.

Acknowledgements

This work has been supported in part by the European Commission through FP7-ICT-IP project PhoxTrot (contract no. 318240) and FP7 MC-IAPP project COMANDER (contract no. 612257).

Author details

T. Alexoudi[1,2*], G.T. Kanellos[2], S. Dris[3], D. Kalavrouziotis[3], P. Bakopoulos[3], A. Miliou[1,2] and N. Pleros[1,2]

*Address all correspondence to: theonial@iti.gr

1 Information & Technologies Institute, Center for Research & Technology Hellas, Thessaloniki, Greece

2 Department of Informatics, Aristotle University of Thessaloniki, Thessaloniki, Greece

3 School of Electrical Engineering and Computer Engineering, National Technical University of Athens, Athens, Greece

References

[1] W. Freude et al. Linear and nonlinear semiconductor optical amplifiers. In: Proceedings of 12th International Conference on Transparent Optical Networks (ICTON 2010); 27 June–1 July; Munich, Germany. IEEE; 2010. p. 1–4. DOI: 10.1109/ICTON.2010.5549097

[2] Dong, X. Zhang, S. Fu, J. Xu, P. Shum and D. Huang. Ultrafast all-optical signal processing based on single semiconductor optical amplifier. Journal of Selected Topics in Quantum Electronics. 2008; 14(3):770–778. DOI: 10.1109/JSTQE.2008.916248

[3] J. Leuthold. All-optical wavelength conversion up to 100 Gbit/s with SOA delayed-interference configuration. OSA Trends in Optics and Photonics. 2000; 44(Optical Amplifiers and Their Applications):OWB3.

[4] Z. Li et al. All-optical logic gates using semiconductor optical amplifier assisted by optical filter. Electronic Letters. 2005; 41(25):1397–1399. DOI: 10.1049/el:20053385

[5] G. Berrettinni, A. Simi, A. Malacarne, A. Bogoni, and L. Potí. Ultrafast integrable and reconfigurable XNOR, AND, NOR and NOT photonic logic gate. IEEE Photonics Technology Letters. 2006; 18(8):917–919. DOI: 10.1109/LPT.2006.873570

[6] A. Hamie, A. Sharaiha, M. Guégan, and B. Puce. All-optical logic NOR gate using two-cascaded semiconductor optical amplifiers. IEEE Photonics Technology Letters. 2002;14(10):1439–1441. DOI: 10.1109/LPT.2002.802426

[7] G. T. Kanellos et al. All-optical 3R burst mode reception at 40 Gb/s using 4 integrated MZI switches. IEEE/OSA Journal of Lightwave Technology. 2007; 25(1):184–192. DOI: 10.1109/JLT.2006.888169

[8] L. Aggazi et al. Monolithic integration of the erbium-doped amplifier with silicon-on-insulator waveguides. OSA Optics Express. 2010;18(26):27703–27711. DOI: 10.1364/OE.18.027703

[9] C.S. Nicholes et al. An 8x8 InP monolithic tunable optical router (MOTOR) packet forwarding chip. IEEE/OSA Journal of Lightwave Technology. 2010;28(4):641–650. DOI: 10.1109/JLT.2009.2030145

[10] V.S. Pato et al. All-optical burst mode power equalizer based on cascaded SOAs for 10-Gb/s EPONs. IEEE Photonics Technology Letters. 2008;20(24):2078–2080. DOI: 10.1109/LPT.2008.2006629

[11] D. Chiaroni et al. Optical packet ring network offering bit rate and modulation formats transparency. In: Proceedings of Optical Fiber Communication (OFC) Conference; 21–25 March; San Diego, CA, USA. IEEE; 2010. p. 1–3. DOI: 10.1364/OFC.2010.OWI3

[12] M. Settembre et al. Cascaded optical communication systems with in-line semiconductor optical amplifiers. IEEE/OSA Journal of Lightwave Technology. 1997; 15(6): 962–967. DOI: 10.1109/50.588666

[13] G.P. Agrawal and N.A. Olsson. Self-phase modulation and spectral broadening of optical pulses in semiconductor laser amplifiers. IEEE Journal of Quantum Electronics. 1989; 25(11):2297–2306. DOI: 10.1109/3.42059

[14] T. Alexoudi, S. Dris, D. Kalavrouziotis, P. Bakopoulos, A. Miliou and N. Pleros. Timing jitter of SOA-amplified intensity modulated optical pulses. In: Optical Fiber Communication Conference (OFC); 4-8 March; Los Angeles, CA, USA. IEEE; 2012. p. 1–3. DOI: 10.1364/NFOEC.2012.JTh2A.13

[15] T. Alexoudi, G.T. Kanellos, S. Dris, D. Kalavrouziotis, P. Bakopoulos, A. Miliou and N. Pleros. Deterministic timing jitter analysis of SOA-amplified intensity modulated optical pulses. IEEE Photonics Journal. 2012; 4(5):1947–1955. DOI: 10.1109/JPHOT.2012.2220341

[16] R. G.-Castrejón and A. Filios. Pattern-effect reduction using a cross-gain modulated holding beam in semiconductor optical in-line amplifier. IEEE/OSA Journal of Lightwave Technology. 2006; 24(12):4912–4917. DOI: 10.1109/JLT.2006.884972

[17] S. Bischoff, M.L. Nielsen and J J. Mork. Improving the all-optical response of SOAs using a modulated holding signal. IEEE/OSA Journal of Lightwave Technology. 2004; 22(5):1303–1308. DOI: 10.1109/JLT.2004.825354

[18] G. T. Kanellos, N. Pleros, C. Bintjas, H. Avramopoulos. SOA-based interferometric optical hard-limiter. In: Proceedings of Optical Amplifiers and their Applications (OAA) Conference; 30 June; San Francisco, CA, USA. OSA; 2004. DOI: 10.1364/IPR.2004.JWB8

[19] K. Vlachos, G. Theophilopoulos, A. Hatziefremidis and H. Avramopoulos. 30 Gbps all-optical, clock recovery circuit. IEEE Photonics Technology Letters. 2000;12(6):705–707. DOI: 10.1109/LPT.2002.801095.

[20] N. Pleros et al. Recipe for intensity modulation reduction in SOA-based interferometric switches. IEEE/OSA Journal of Lightwave Technology. 2004;22(12):2834–2841. DOI: 10.1109/JLT.2004.834834

[21] S.V. Kartalopoulos et al. Optical bit error rate: an estimation methodology. 1st ed. Willey-IEEE Press; 2004. 291 p. ISBN: 978-0-471-61545-3

[22] J. Peatross, S.A. Glasgow and M. Ware. Average energy flow of optical pulses in dispersive media. APS Physics Review Letters. 2000;84(11):2370–2373. DOI: http://dx.doi.org/10.1103/PhysRevLett.84.2370

[23] R. Stephens. Analyzing jitter at high data rates. IEEE Communications Magazine. 2004; 42(2):S6–10. DOI: 10.1109/MCOM.2003.1267095

[24] Agilent Technologies. Measuring jitter in digital systems, application note 1448-1 [Internet]. 1 June 2003. Available from http://www.colbyinstruments.com/pdfs/5988-9109EN.pdf [Accessed: 31-5-2015]

[25] Maxim Integrated. Converting between RMS to peak-to-peak Jitter at a specified BER, application note 462 HFAN-04.0.2 [Internet]. 2008 [Updated: 04/2008]. Available from: http://pdfserv.maximintegrated.com/en/an/AN462.pdf [Accessed: 31-5-2015]

IntechOpen